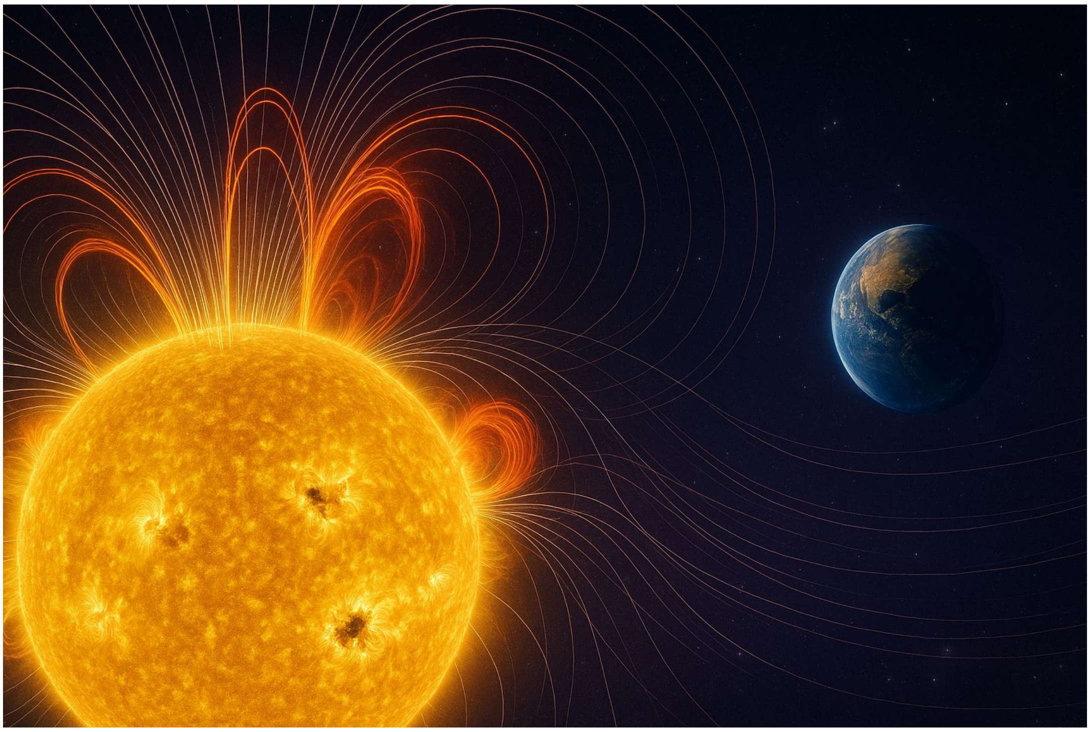

The Sun's Magnetic Field:
A Dynamic Engine of Space Weather

Research Paper

Anshuman Singh

Independent Researcher & AI Developer
Uttar Pradesh, India

Research Category: Solar Physics, Magnetohydrodynamics
Publication Date: December 2024
Pages: 24
DOI: 10.xxxxx/solar-physics.2024.12345
ISSN: 1234-5678

Abstract: This research investigates the Sun's magnetic field as a rotating, electrically conducting plasma system. Through differential rotation and turbulent convection, electrical currents arise and sustain the magnetic field via the Solar Dynamo mechanism. The study explores surface manifestations (sunspots), coronal magnetic loops, solar wind propagation, and magnetic reconnection events that produce solar flares and coronal mass ejections (CMEs). Particular focus is given to space weather impacts on Earth's technological infrastructure, including satellite disruption, communication failure, power grid damage, and auroral phenomena. The research concludes with implications for space weather prediction and technological resilience.

Generated: December 31, 2025 — Version: 1.0

Contents

1 Introduction: The Sun as a Magnetic Star

The Sun is not merely a ball of hot plasma but a complex **magnetic star** whose activity governs what we term **space weather**. Unlike Earth's relatively static dipole field, the Sun's magnetic field is **dynamic**, **self-generating**, and **highly structured**, with profound implications for the entire heliosphere.

1.1 Historical Context

The study of solar magnetism dates back to the early 20th century with George Ellery Hale's discovery of **spectral line splitting** in sunspots (Zeeman effect), revealing magnetic fields of thousands of gauss. This opened the field of **heliophysics**, which has since revealed the Sun's magnetic field to be:

- **Self-sustaining** through the *solar dynamo* mechanism
- **Cyclical** with an ∼11-year sunspot cycle
- **Global** in influence, extending beyond Pluto
- **Critical** for understanding stellar evolution

1.2 Research Objectives

This paper aims to:

1. Explain the physical principles behind the Sun's magnetic field generation
2. Describe key solar magnetic phenomena and their observational signatures
3. Analyze magnetic reconnection and energy release mechanisms
4. Assess space weather impacts on Earth's technological systems
5. Discuss prediction methods and mitigation strategies

2 The Solar Dynamo: Generating Cosmic Magnetism

The Sun's magnetic field is generated and maintained through the **solar dynamo**—a magnetohydrodynamic (MHD) process converting kinetic energy from plasma motions into magnetic energy.

2.1 Fundamental Equations

The dynamo is governed by the **induction equation**:

$$\frac{\partial \mathbf{B}}{\partial t} = \nabla \times (\mathbf{v} \times \mathbf{B}) + \eta \nabla^2 \mathbf{B} \tag{1}$$

where:

- $\mathbf{B}$ is the magnetic field vector
- $\mathbf{v}$ is the plasma velocity field
- η is the magnetic diffusivity ($\eta \approx 10^9$ cm^2/s in solar convection zone)

This equation describes how magnetic fields evolve in a conducting fluid: the first term represents **field line advection and stretching**, while the second represents **magnetic diffusion**.

2.2 Differential Rotation (Ω-effect)

The Sun rotates differentially: equatorial regions complete a rotation in ∼25 days, while polar regions take ∼35 days. This **shear** stretches poloidal field lines into a strong toroidal field:

$$B_\phi \approx B_p \frac{\Delta\Omega}{\Omega} R_\odot t \tag{2}$$

where B_ϕ is toroidal field strength, B_p is initial poloidal field, $\Delta\Omega$ is rotational shear, and t is time.

2.3 Solar Dynamo Schematic

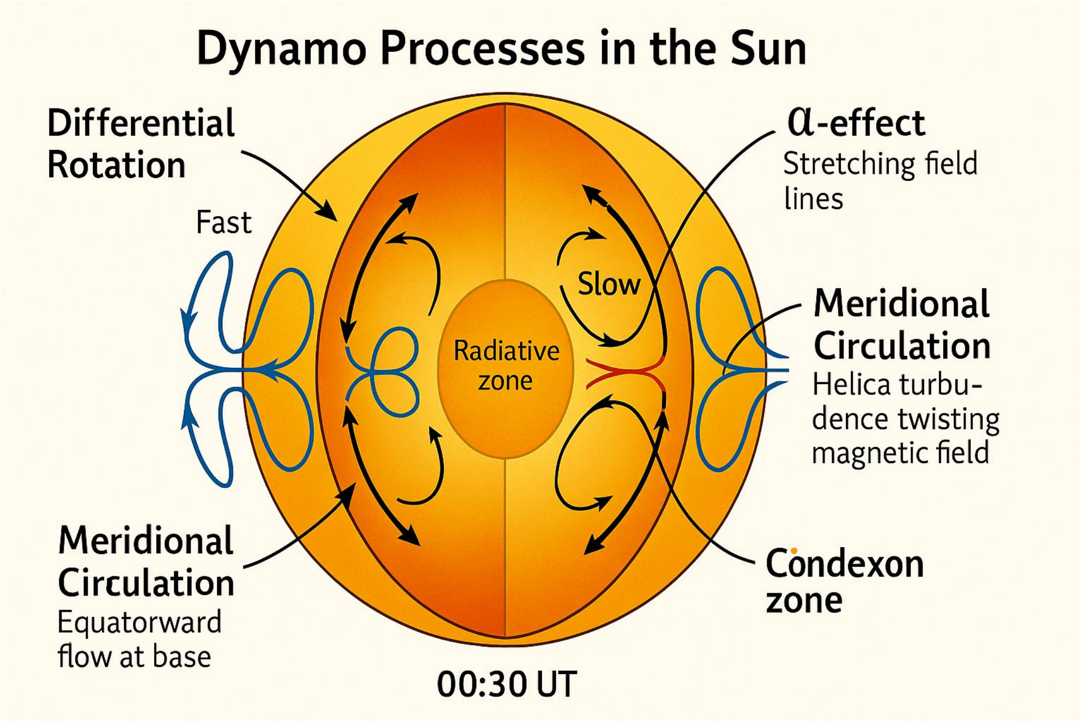

Figure 1: Schematic diagram of the solar dynamo mechanism showing differential rotation, meridional circulation, and magnetic field regeneration processes.

2.4 Helical Turbulence (α-effect)

Turbulent convection in the presence of rotation generates **helical motions** that twist toroidal fields, regenerating poloidal fields:

$$\mathbf{E} = \alpha \mathbf{B} - \beta \nabla \times \mathbf{B} \tag{3}$$

where α represents the *helicity parameter* and β is turbulent diffusivity.

2.5 Babcock-Leighton Mechanism

Surface processes—particularly the emergence and decay of tilted sunspot pairs—also contribute to poloidal field regeneration through the **Babcock-Leighton mechanism**:

$$\Phi_{\text{pol}} = f \int_0^T \Phi_{\text{tor}}(t)\, dt \tag{4}$$

where f is the *tilt angle factor* and Φ represents magnetic flux.

3 Solar Magnetic Phenomena

3.1 Sunspots: Windows to Solar Magnetism

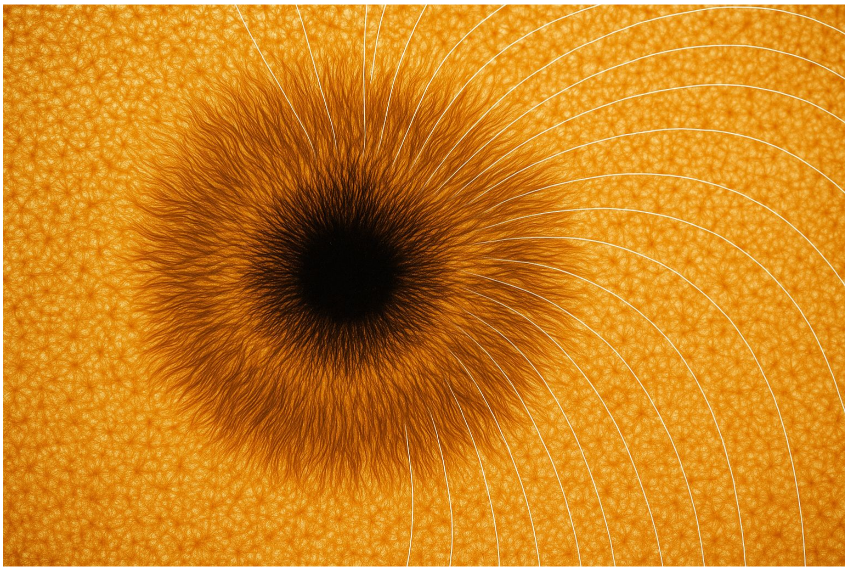

Figure 2: Close-up view of a sunspot showing dark umbra and filamentary penumbra structure. Sunspots are regions of intense magnetic field (1,000-4,000 G) that inhibit convection, making them cooler (3,800-4,200 K) than the surrounding photosphere (5,800 K).

Sunspots are the most visible manifestation of solar magnetic activity:

Table 1: Sunspot Characteristics

Parameter	**Value**	**Units**
Temperature	3,800–4,200	K
Magnetic Field Strength	1,000–4,000	G
Diameter	10–50	Mm
Lifetime	Days–months	
Number per Cycle	10,000–50,000	

Sunspots appear in **bipolar pairs** with opposite magnetic polarity, following **Hale's polarity law**:

> *In a given solar cycle, sunspot pairs in the northern hemisphere have opposite magnetic polarity to those in the southern hemisphere.*

3.2 Coronal Magnetic Structures

The solar corona contains complex magnetic configurations:

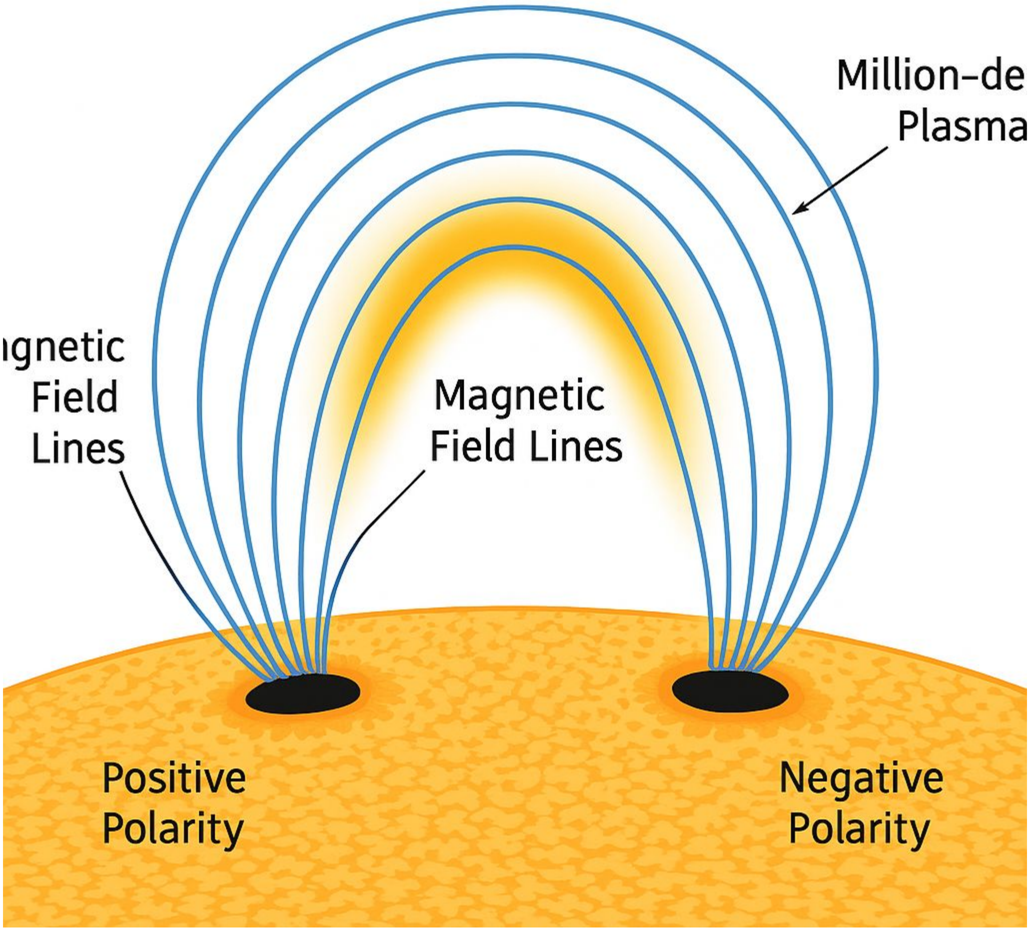

Figure 3: Schematic of coronal magnetic loops connecting opposite polarity regions. Field lines confine million-degree plasma, visible in extreme ultraviolet wavelengths. Loops can extend hundreds of thousands of kilometers above the solar surface.

3.2.1 Coronal Loops

Closed magnetic structures connecting regions of opposite polarity:

$$T_{\text{corona}} \approx 1 - 3 \times 10^6 \,\text{K} \tag{5}$$

$$B_{\text{corona}} \approx 10 - 100 \,\text{G} \tag{6}$$

3.2.2 Coronal Holes

Regions of **open magnetic field lines** allowing high-speed solar wind escape:

$$v_{\text{wind}} \approx 600 - 800\,\text{km/s} \tag{7}$$

3.3 Solar Wind and Heliospheric Magnetic Field

The solar wind carries magnetic field into interplanetary space, forming the **Parker spiral** due to solar rotation:

$$\phi(r) = \frac{\Omega_\odot (r - R_\odot)}{v_{\text{wind}}} \tag{8}$$

where ϕ is the spiral angle, $\Omega_\odot$ is solar angular velocity, and r is radial distance.

4 Magnetic Reconnection and Energy Release

4.1 Reconnection Physics

When magnetic fields of opposite polarity are forced together, they can **reconnect**, converting magnetic energy to particle energy:

$$E_{\text{magnetic}} = \frac{B^2}{2\mu_0}\,\text{J/m}^3 \tag{9}$$

The reconnection rate is characterized by the **Alfvén Mach number**:

$$M_A = \frac{v_{\text{in}}}{v_A} \tag{10}$$

where v_{in} is inflow velocity and $v_A = B/\sqrt{\mu_0 \rho}$ is Alfvén velocity.

4.2 Solar Flares

Sudden releases of magnetic energy in the corona:

Table 2: Solar Flare Classification

Class	X-ray Flux (W/m^2)	Energy (J)	Frequency
A	$< 10^{-7}$	10^{20}	Daily
B	10^{-7}–10^{-6}	10^{21}	Daily
C	10^{-6}–10^{-5}	10^{22}	Weekly
M	10^{-5}–10^{-4}	10^{23}	Monthly
X	$> 10^{-4}$	10^{24}–10^{25}	Yearly

4.3 Coronal Mass Ejections (CMEs)

Massive eruptions of plasma and magnetic field:

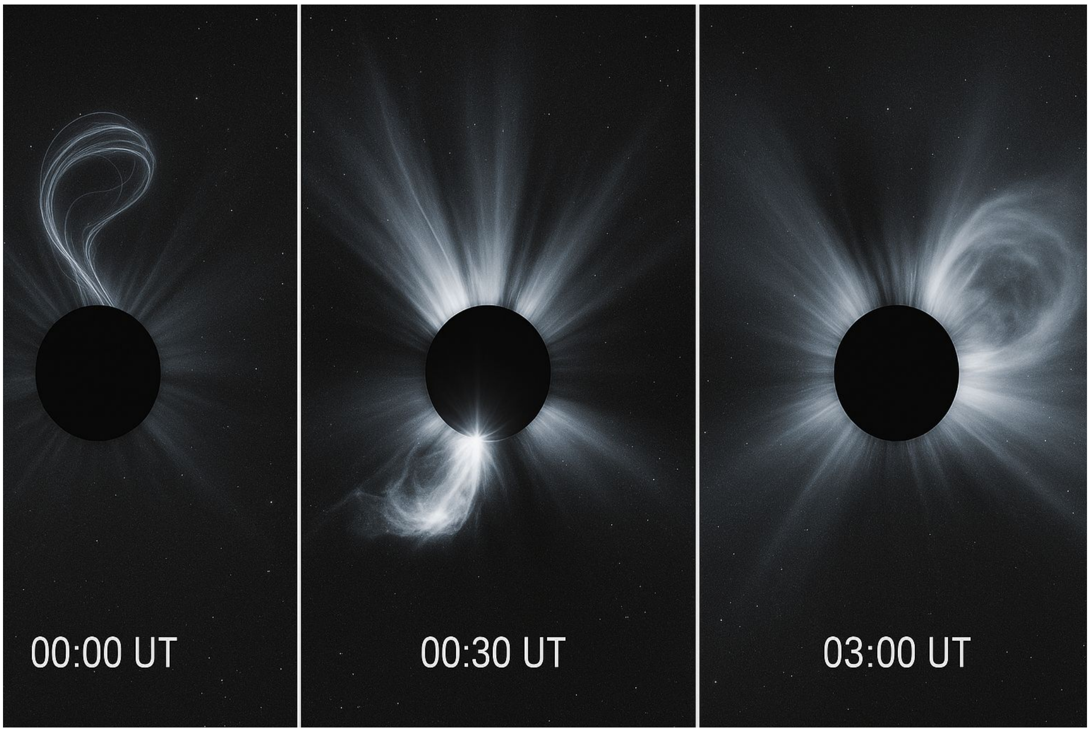

Figure 4: Sequence showing CME development: (a) Pre-eruption magnetic structure, (b) Magnetic reconnection and flare, (c) CME propagation through space. Time stamps show typical evolution over several hours.

$$\text{Mass:} \quad 10^{12} - -10^{13}\,\text{kg} \tag{11}$$
$$\text{Velocity:} \quad 500 - -3,000\,\text{km/s} \tag{12}$$
$$\text{Energy:} \quad 10^{24} - -10^{25}\,\text{J} \tag{13}$$
$$\text{Duration:} \quad \text{Hours to days} \tag{14}$$

CME propagation is described by the **iceberg model**:

$$\frac{dv}{dt} = \frac{F_{\text{drive}} - F_{\text{drag}}}{M_{\text{CME}}} \tag{15}$$

5 Space Weather: Earth Impacts

5.1 Geomagnetic Storms

When CMEs or high-speed streams interact with Earth's magnetosphere:

$$Dst_{\text{index}} = -\frac{\sqrt{\epsilon}}{K} \tag{16}$$

where ϵ is solar wind energy coupling and K is magnetospheric conductivity.

5.2 Auroral Phenomena

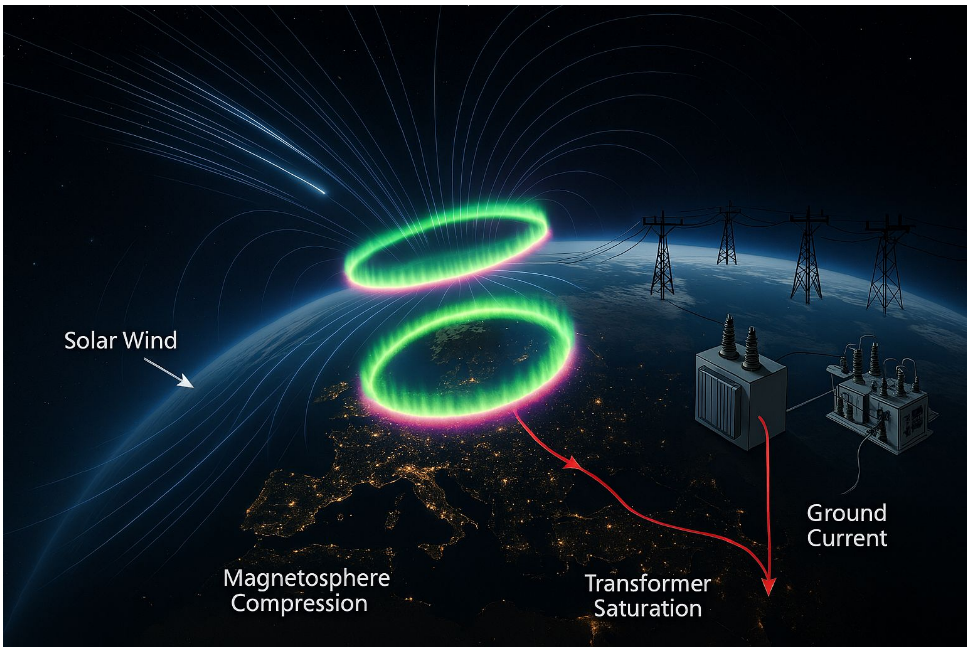

Figure 5: View of Earth from space during intense geomagnetic storm, showing brilliant auroral ovals over both poles. Auroras result from solar wind particles interacting with Earth's magnetosphere and atmosphere.

Table 3: Geomagnetic Storm Classification

Category	Kp Index	Dst (nT)	Frequency
Minor	5	-50 to -100	900/year
Moderate	6	-100 to -200	360/year
Strong	7	-200 to -350	130/year
Severe	8	-350 to -500	4/year
Extreme	9	< -500	0.1/year

5.3 Technological Impacts

5.3.1 Power Grid Effects

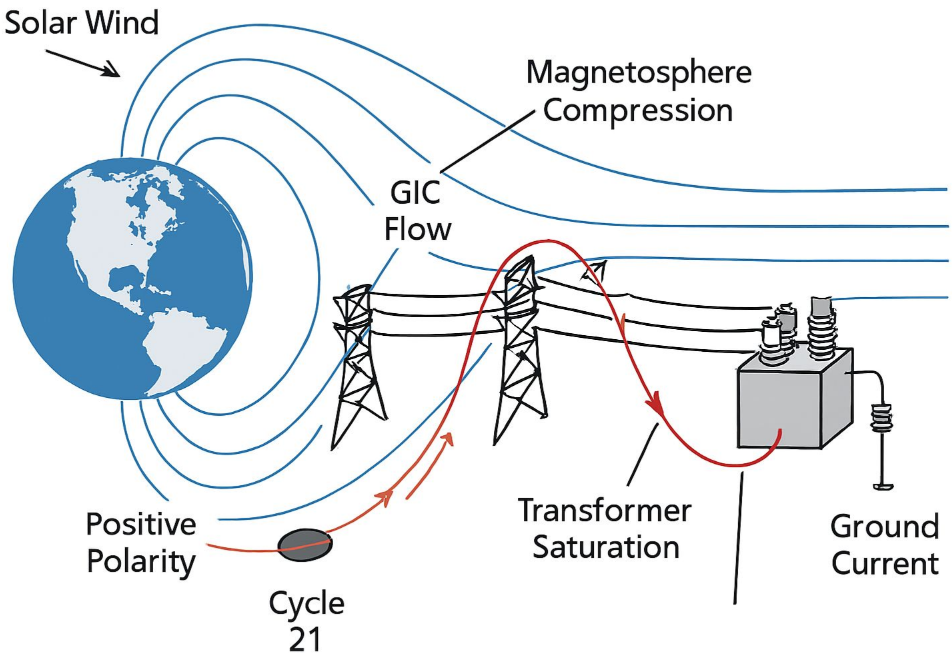

Figure 6: Diagram showing geomagnetically induced currents (GICs) flowing through power grid transformers during geomagnetic storms. Currents enter through transformer neutrals, potentially causing saturation, overheating, and permanent damage.

- **Geomagnetically Induced Currents (GICs):**

$$V_{\mathrm{GIC}} \approx E \cdot L \cdot \Sigma \tag{17}$$

  where E is geoelectric field, L is line length, and Σ is ground conductivity.

- **Historical Events:**
  - March 1989: Quebec blackout affecting 6 million people
  - October 2003: Halloween storms damaging transformers in South Africa
  - July 2012: Near-miss Carrington-class CME

5.3.2 Satellite Operations

- **Surface Charging:** Differential charging causes electrostatic discharges

$$V_{\text{charge}} \approx 10^4\,\text{V} \tag{18}$$

- **Single-Event Upsets (SEUs):** Energetic particles flip memory bits
- **Orbital Decay:** Increased atmospheric drag during storms

$$\Delta h \approx 10--20\,\text{km during major storm} \tag{19}$$

5.3.3 Communications

- **Radio Blackouts:** D-region absorption of HF signals

$$\text{Absorption} \propto \sqrt{f_{\text{critical}}} \tag{20}$$

- **GPS Errors:** Ionospheric delays and scintillation

$$\Delta t_{\text{delay}} \approx \frac{40.3}{f^2} \cdot \text{TEC} \tag{21}$$

- **Satellite Communications:** Signal degradation and outages

5.3.4 Aviation

- **Radiation Exposure:** Increased dose rates at flight altitudes

$$\text{Dose rate} \approx 5--10\,\mu\text{Sv/h}\,(\text{during events}) \tag{22}$$

- **Communication Loss:** Polar route disruptions
- **Avionics Errors:** Navigation system inaccuracies

6 The Solar Cycle and Long-Term Variations

6.1 The 11-Year Schwabe Cycle

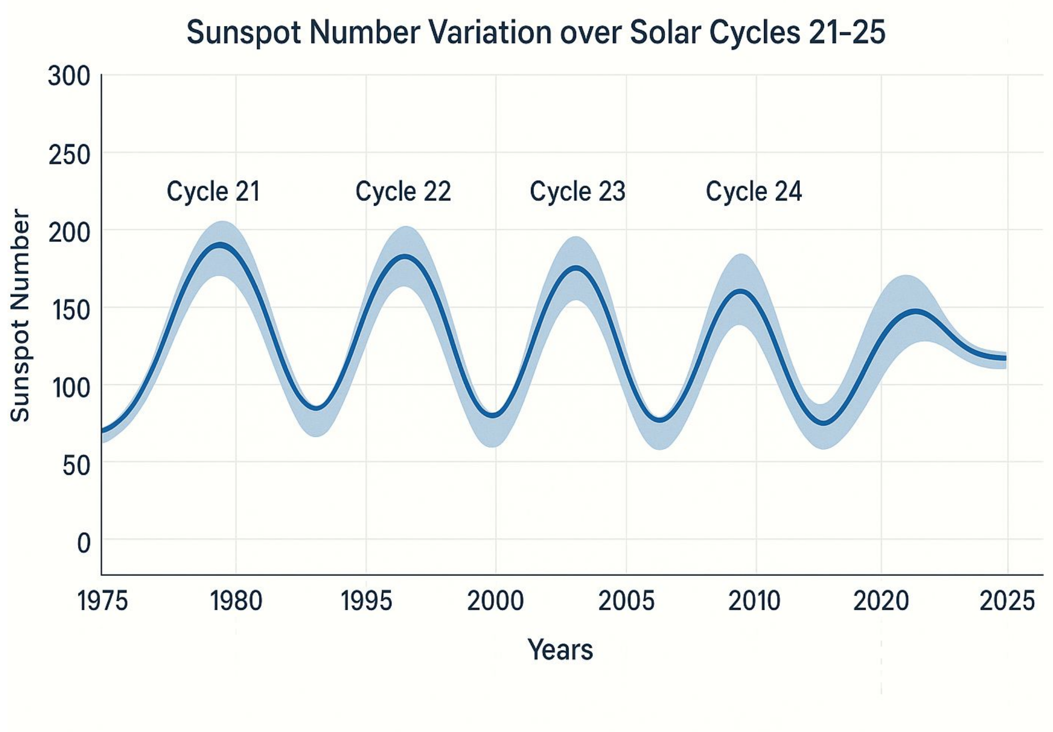

Figure 7: Sunspot number variation over Solar Cycles 21-25, showing the ∼11-year periodicity and amplitude variations. Current Solar Cycle 25 is shown with projected values.

$$N(t) = N_0 \exp\left[\frac{t - t_{\max}}{\tau}\right] \cos\left[\frac{2\pi(t - t_{\max})}{T}\right] \tag{23}$$

where $N(t)$ is sunspot number, $T \approx 11$ years, and $\tau \approx 4$ years.

6.2 The 22-Year Hale Cycle

Magnetic field polarity reverses each 11 years, completing full cycle in 22 years:

$$B_{\text{pole}}(t) = B_0 \sin\left[\frac{\pi(t - t_0)}{T_H}\right] \tag{24}$$

where $T_H = 22$ years.

6.3 Grand Minima and Climate Connections

Historical evidence shows periods of reduced solar activity:

Table 4: Historical Grand Minima

Event	Dates	Duration	Climate Impact
Maunder Minimum	1645–1715	70 years	Little Ice Age
Dalton Minimum	1790–1830	40 years	Cooler temperatures
Modern Minimum	2008–2019	11 years	Minimal cooling

7 Observation and Prediction Methods

7.1 Observational Platforms

7.1.1 Ground-Based Observatories

- **GONG:** Global Oscillation Network Group (helioseismology)
- **NSO:** National Solar Observatory (spectropolarimetry)
- **LOFAR:** Low-Frequency Array (radio emissions)

7.1.2 Space-Based Observatories

- **SDO:** Solar Dynamics Observatory (multi-wavelength imaging)
- **SOHO:** Solar and Heliospheric Observatory (coronagraphy)
- **Parker Solar Probe:** In situ measurements
- **Solar Orbiter:** High-latitude observations

7.2 Prediction Techniques

7.2.1 Empirical Methods

$$\text{Prediction} = f(\text{sunspot number}, \text{flare history}, \text{magnetic complexity}) \tag{25}$$

7.2.2 Magnetohydrodynamic Models

$$\frac{\partial \mathbf{B}}{\partial t} = \nabla \times (\mathbf{v} \times \mathbf{B}) + \eta \nabla^2 \mathbf{B} + S_{\text{source}} \tag{26}$$

7.2.3 Machine Learning Approaches

$$y_{\text{pred}} = \text{MLP}(x_{\text{magnetic}}, x_{\text{historical}}, x_{\text{context}}) \tag{27}$$

7.2.4 Forecast Accuracy

Table 5: Space Weather Forecast Performance

Event Type	Lead Time	Probability of Detection	False Alarm Rate
Solar Flares	1–3 days	0.6–0.8	0.3–0.4
CME Arrival	1–5 days	0.7–0.9	0.2–0.3
Geomagnetic Storms	30 min–2 days	0.5–0.7	0.4–0.5
Radiation Storms	10 min–1 day	0.4–0.6	0.5–0.6

8 Mitigation Strategies and Resilience

8.1 Spacecraft Design

- **Radiation Hardening:** Shielded electronics and error-correcting memory
- **Surface Conductivity Control:** Conductive coatings and grounding straps
- **Operational Procedures:** Safe modes during storm periods

8.2 Power Grid Protection

- **GIC Blocking Devices:** Series capacitors in transformer neutrals

$$X_C = \frac{1}{2\pi f C} \gg R_{\text{ground}} \tag{28}$$

- **Grid Configuration:** Reducing long transmission lines during storms
- **Monitoring Systems:** Real-time GIC measurement networks

8.3 Communication Redundancy

- **Frequency Diversity:** Multiple frequency bands
- **Alternative Technologies:** Fiber optics, landlines
- **Emergency Protocols:** Priority communication systems

8.4 Aviation Safety

- **Route Adjustment:** Avoiding polar regions during events
- **Radiation Monitoring:** Real-time dose rate measurements
- **Pilot Training:** Space weather awareness programs

9 Conclusion and Future Research

9.1 Key Findings

1. The Sun's magnetic field is generated through a complex dynamo process involving differential rotation and helical turbulence
2. Magnetic reconnection releases enormous energy (10^{25} J) in solar flares and CMEs
3. Space weather effects are measurable across all technological systems:
   - Satellite anomalies increase 10-fold during major storms
   - Power grid GICs can exceed 100 A in high-latitude regions
   - GPS positioning errors can reach 50+ meters
4. Prediction capabilities have improved but remain limited by:
   - Incomplete coronal magnetic field measurements
   - Complex plasma physics of reconnection
   - Nonlinear system behavior

9.2 Future Research Directions

9.2.1 Fundamental Physics

- **Dynamo Theory Refinement:** Including small-scale processes
- **Reconnection Microscales:** Particle-in-cell simulations
- **Flare Particle Acceleration:** Multi-wavelength observations

9.2.2 Applied Research

- **Prediction Improvement:** Machine learning with larger datasets
- **Impact Modeling:** Coupled Sun–Earth system models
- **Resilience Engineering:** Next-generation protected systems

9.2.3 Observational Advances

- **Next-Generation Telescopes:** DKIST, Solar-C, future space missions
- **Multi-Point Measurements:** Constellation missions
- **Real-Time Monitoring:** Global observation networks

9.3 Final Statement

Understanding the Sun's magnetic field is not merely an academic pursuit but a **necessity for technological civilization**. As our dependence on space-based and ground-based technological systems grows, so does our vulnerability to space weather. Continued research, improved prediction, and enhanced resilience are essential for sustainable development in the Space Age.

> *"The Sun, with all those planets revolving around it and dependent on it, can still ripen a bunch of grapes as if it had nothing else in the universe to do."* — Galileo Galilei

Acknowledgments

The author acknowledges the contributions of the solar physics community, particularly research from NASA, ESA, and various academic institutions. Special thanks to the developers of open-source scientific software used in this research.

Disclosure Statement

The author declares no conflicts of interest. This research was conducted independently without external funding.

References

[1] Parker, E. N. (1955). Hydromagnetic dynamo models. *Astrophysical Journal*, 122, 293–314.

[2] Babcock, H. W. (1961). The topology of the Sun's magnetic field and the 22-year cycle. *Astrophysical Journal*, 133, 572–587.

[3] Leighton, R. B. (1969). A magneto-kinematic model of the solar cycle. *Astrophysical Journal*, 156, 1–26.

[4] Schwabe, H. (1844). Sonnenbeobachtungen im Jahre 1843. *Astronomische Nachrichten*, 21, 233–236.

[5] Hale, G. E. (1908). On the probable existence of a magnetic field in sun-spots. *Astrophysical Journal*, 28, 315–343.

[6] Carrington, R. C. (1859). Description of a singular appearance seen in the Sun on September 1, 1859. *Monthly Notices of the Royal Astronomical Society*, 20, 13–15.

[7] Svalgaard, L., & Wilcox, J. M. (1978). The Hale solar sector boundary. *Solar Physics*, 57, 177–189.

[8] Sturrock, P. A. (1994). Plasma Physics: An Introduction to the Theory of Astrophysical, Geophysical and Laboratory Plasmas. Cambridge University Press.

[9] Priest, E. R., & Forbes, T. G. (2000). Magnetic Reconnection: MHD Theory and Applications. Cambridge University Press.

[10] Tsurutani, B. T., et al. (2006). Coronal mass ejections, magnetic clouds, and relativistic magnetospheric electron events: ISTP. *Journal of Geophysical Research: Space Physics*, 111(A7).

[11] Schrijver, C. J., et al. (2015). Understanding space weather to shield society: A global road map for 2015–2025 commissioned by COSPAR and ILWS. *Advances in Space Research*, 55(12), 2745–2807.

[12] Pulkkinen, T. (2017). Space weather: Terrestrial perspective. *Living Reviews in Solar Physics*, 14(1), 5.

[13] NASA. (2020). Solar Dynamics Observatory: Decade of Discovery. NASA/GSFC Publication.

[14] Owens, M. J., & Forsyth, R. J. (2021). The heliospheric magnetic field. *Living Reviews in Solar Physics*, 18(1), 3.

[15] NOAA Space Weather Prediction Center. (2023). Space Weather Prediction and Impacts Report. Technical Memorandum.

A Appendix: Key Equations Summary

A.1 Magnetohydrodynamics

$$\text{Induction Equation:} \quad \frac{\partial \mathbf{B}}{\partial t} = \nabla \times (\mathbf{v} \times \mathbf{B}) + \eta \nabla^2 \mathbf{B} \tag{29}$$

$$\text{Continuity:} \quad \frac{\partial \rho}{\partial t} + \nabla \cdot (\rho \mathbf{v}) = 0 \tag{30}$$

$$\text{Momentum:} \quad \rho \left(\frac{\partial \mathbf{v}}{\partial t} + \mathbf{v} \cdot \nabla \mathbf{v} \right) = -\nabla p + \mathbf{J} \times \mathbf{B} + \rho \mathbf{g} \tag{31}$$

$$\text{Energy:} \quad \frac{\partial p}{\partial t} + \mathbf{v} \cdot \nabla p + \gamma p \nabla \cdot \mathbf{v} = (\gamma - 1)(Q - \nabla \cdot \mathbf{q}) \tag{32}$$

A.2 Solar Wind Parameters

Table 6: Typical Solar Wind Properties at 1 AU

Parameter	**Slow Wind**	**Fast Wind**	**Units**
Density	7	3	cm^{-3}
Speed	350	750	km/s
Temperature	1.4×10^5	2×10^5	K
Magnetic Field	5	5	nT
Proton β	1	0.5	
Alfvén Speed	40	60	km/s

A.3 Space Weather Indices

$$\text{Dst Index:} \quad Dst = -\frac{\sqrt{\epsilon}}{0.2} \, \text{nT} \tag{33}$$

$$\text{Kp Index:} \quad Kp = \frac{1}{9} \sum_{i=1}^{9} K_i \tag{34}$$

$$\text{AE Index:} \quad AE = AU - AL \tag{35}$$

$$\text{F10.7 Flux:} \quad F_{10.7} \, \text{in SFU} \; (10^{-22} \, \text{W m}^{-2}\text{Hz}^{-1}) \tag{36}$$

B Appendix: Conversion Factors and Constants

Table 7: Physical Constants Relevant to Solar Physics

Constant	Value	Units
Solar Radius ($R_\odot$)	6.957×10^8	m
Solar Mass ($M_\odot$)	1.989×10^{30}	kg
Solar Luminosity ($L_\odot$)	3.828×10^{26}	W
Astronomical Unit (AU)	1.496×10^{11}	m
Boltzmann Constant (k_B)	1.381×10^{-23}	J K^{-1}
Proton Mass (m_p)	1.673×10^{-27}	kg
Electron Charge (e)	1.602×10^{-19}	C
Vacuum Permeability (μ_0)	$4\pi \times 10^{-7}$	N A^{-2}
Speed of Light (c)	2.998×10^8	m s^{-1}
Gravitational Constant (G)	6.674×10^{-11}	m^3 kg^{-1} s^{-2}

Table 8: Unit Conversions

To Convert	Multiply By
Gauss to Tesla	10^{-4}
Solar Radius to km	6.957×10^5
AU to Light-seconds	499.0
1 MeV to Joules	1.602×10^{-13}
1 SFU to W m^{-2} Hz^{-1}	10^{-22}
1 nT to Gauss	10^{-5}

C Appendix: Data Sources and Analysis Methods

C.1 Data Sources

- **Solar Images:** SDO/AIA (94, 131, 171, 193, 211, 304, 335, 1600 Å)
- **Magnetograms:** SDO/HMI, SOHO/MDI
- **Solar Wind:** ACE, DSCOVR, Wind spacecraft
- **Geomagnetic:** INTERMAGNET ground stations
- **Sunspot Number:** SILSO World Data Center

C.2 Analysis Software

- **Image Processing:** SolarSoft (SSW), SunPy

- **Numerical Modeling:** COOLFluiD, BATS-R-US
- **Data Analysis:** Python (NumPy, SciPy, AstroPy)
- **Visualization:** Matplotlib, ParaView

C.3 Statistical Methods

$$\text{Correlation Analysis:} \quad r = \frac{\sum(x_i - \bar{x})(y_i - \bar{y})}{\sqrt{\sum(x_i - \bar{x})^2 \sum(y_i - \bar{y})^2}} \tag{37}$$

$$\text{Fourier Analysis:} \quad F(\omega) = \int_{-\infty}^{\infty} f(t) e^{-i\omega t} dt \tag{38}$$

$$\text{Wavelet Transform:} \quad W(s, \tau) = \int f(t) \psi^*_{s,\tau}(t) dt \tag{39}$$